Bioconjugate Chemistry

Article

Cite This: Bioconjugate Chem. 2019, 30, 3069−3077

pubs.acs.org/bc

Versatile Reversible Cross-Linking Strategy to Stabilize CCMV Virus Like Particles for Efficient *siRNA* Delivery

Chiara Pretto and Jan C. M. van Hest*

Eindhoven University of Technology, Institute for Complex Molecular Systems, PO Box 513, 5600 MB Eindhoven, The Netherlands

Supporting Information

ABSTRACT: Virus like particles obtained from the Cowpea Chlorotic Mottle Virus (CCMV) represent an innovative platform for drug delivery applications. Their unique reversible self-assembly properties as well as their suitability for both cargo loading and functionalization make them a versatile scaffold for numerous purposes. One of the main drawbacks of this platform is however its limited stability at physiological conditions. Herein, we report the development of a general reversible cross-linking strategy involving the homobifunctional cross-linker DTSSP (3,3′-dithiobis (sulfosuccinimidylpropionate)) which is suitable for particle stabilization. This methodology is adaptable to different CCMV variants in the presence or absence of a stabilizing cargo without varying neither particle shape nor size thus extending the potential use of these protein cages in nanomedical applications. Cross-linked particles are stable at neutral pH and 37 °C and they are capable of protecting loaded cargo against enzymatic digestion. Furthermore, the reversible nature of the cross-linking ensures particle disassembly when they are taken up by cells. This was demonstrated via the highly effective delivery of active siRNA into cells.

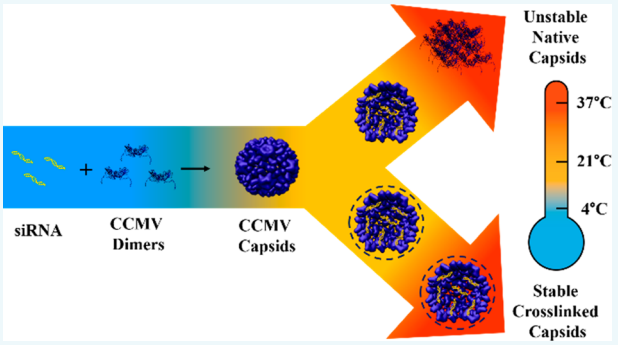

INTRODUCTION

Nanomedicine is one of the leading research directions in the field of drug delivery. A wide range of novel nanocarrier systems has been developed over the years to optimize delivery efficiency, improve release profiles and achieve specific targeting to minimize both dosages and side effects, thus improving patients' quality of life. Several well-studied nanoplatforms include polymeric nanoparticles and conjugates, dendrimers, lipid-based nanoparticles, metal clusters, and protein cages.[1] All of these drug delivery scaffolds have unique properties that make them suitable for specific purposes. Among them, virus like particles (VLP) have recently attracted attention.[2,3] They are mostly based on the protein mantle of regular plant viruses, without the genetic material present. As such, they are robust protein assemblies with a well-defined shape and ordered architecture.[4−6] These systems are biocompatible and biodegradable with a low toxicity profile and their immunogenic response can be reduced by PEGylating the particle surface.[7] An important class of VLPs are the capsids of the Cowpea Chlorotic Mottle Virus (CCMV), which have been extensively studied for their applicability in drug, and especially gene delivery.[8−10] This protein-based platform is derived from a plant RNA virus composed of 180 identical protein subunits (CP) organized to form an icosahedral shell surrounding the central RNA. Nanoparticles are spherical with an external diameter of 28 nm and a smaller internal diameter of 18 nm.[11,12] The most promising feature of this system is its reversible assembly properties at physiological conditions, even in the absence of the viral RNA.[13−15] Indeed, CCMV capsids are able to disassemble at pH 7.5 and reassemble into $T = 3$ particles (Caspar-Klug triangulation number) via a pH reduction of the environment in which they are located. This process can be performed both for wildtype particles after removal of the viral RNA or for recombinantly expressed capsid proteins. Although empty CCMV capsids are stable in slightly acidic conditions, they undergo disassembly into dimers at neutral pH. This reversible behavior is useful for cargo loading, but on the other hand, it reduces applications at physiological conditions. Several methods have been used to achieve capsid stability at neutral pH. The replacement of the original viral RNA with specific genetic material or negatively charged (bio)-polymers allows for electrostatic stabilization. This behavior is strongly associated with the conformational features of the capsid protein. While the C-terminus (residues 176−190) is exposed on the outer surface of the capsid playing a crucial role in particle swelling, the N-terminus faces the inner cavity and its arginine-rich binding domain (ARD, residues 1−25) guarantees electrostatic interaction with negatively charged macromolecules, being essential for cargo-induced particle formation at neutral pH.[16−18] Besides exploitation of negatively charged cargo loading,[19−23] the CCMV capsid can be stabilized

Received: October 31, 2019
Revised: November 22, 2019
Published: November 25, 2019

DOI: 10.1021/acs.bioconjchem.9b00731
Bioconjugate Chem. 2019, 30, 3069−3077

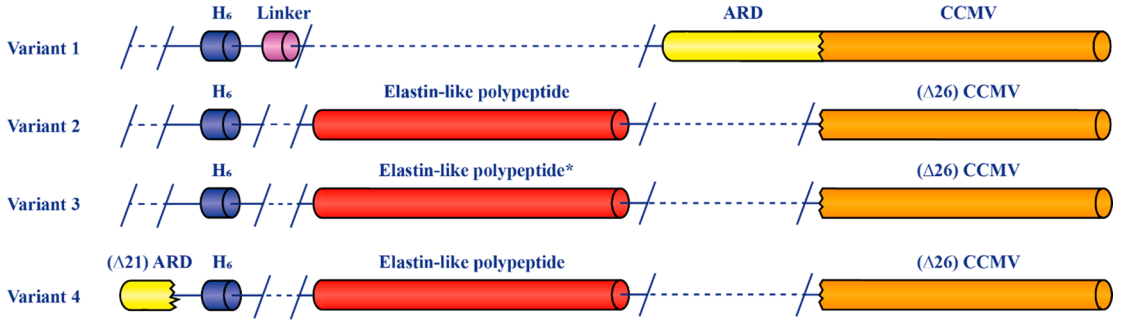

Figure 1. Schematic representation of CCMV variants. All variants have a histidine tag (H_6) for protein purification. Variant 1 (V1) contains a small linker followed by the complete native CCMV sequence. All remaining variants (V2, V3, and V4) have a truncated CCMV sequence missing the arginine-rich RNA-binding domain (ARD, Δ26). While variant 3 (V3) only contains a point mutation in the ELP-sequence (*) consisting of a leucine to arginine substitution, variant 4 (V4) contains part of the ARD (Δ21) which is introduced at the beginning of the protein sequence.

internally by adding metal ions such as nickel, which are able to interact with the histidine tag of recombinantly expressed capsid proteins.[24,25] Another strategy exploits the N-terminal extension with an elastin-like polypeptide (ELP).[26−28] This thermosensitive polymer (with sequence Val-Pro-Gly-Xaa-Gly where Xaa represents any natural amino acid except proline) is capable of switching from a hydrophilic and extended conformation to a hydrophobic and collapsed one, according to a temperature increase as well as an increment of the salt concentration in solution. Even though these techniques have improved capsid applicability as enzymatic delivery systems or nanoreactors,[29−31] cargo-induced assembly exploiting small biologically relevant molecules such as oligonucleotides still represents a challenge and the crucial role of their length in particle assembly has already been established.[32−34] In particular, while the electrostatic interaction between negatively charged cargo and the positively charged ARD of the N-terminus is guaranteed with long DNA or RNA molecules, shorter strands composed of few nucleotides showed to be less efficient in providing this stabilizing effect. In order to overcome this problem we here report on an innovative and versatile strategy for capsid stabilization exploiting the cross-linking agent DTSSP (3,3′-dithiobis-(sulfosuccinimidylpropionate)). This homobifunctional cross-linker has been successfully used to cross-link the external shell of different capsid variants. Because of its disulfide bond the cross-linking is reversed when the capsids are exposed to a reducing environment, as can be found in the cell. The reversible cross-linking neither disrupts particle structure nor functionality of the cargo. We elucidate on this stabilizing mechanism and we present an important application related to gene delivery. CCMV particles loaded with siRNA and cross-linked on their surface are effectively used for in vitro experiments. The achievement of a stable formulation at neutral pH and 37 °C allows us to prove their suitability as gene delivery systems.

RESULTS AND DISCUSSION

Cross-Linking Reaction on Virus Like Particles. Previously, the effect of ssDNA length on CCMV particle assembly was reported.[32] Short strands of DNA and RNA are less prone to guarantee particle stabilization as a result of their lower electrostatic interaction with the positively charged N-terminus of the capsid protein. In particular, it was found that a minimum length of 14 nucleotides is required for particle formation at neutral pH with incubation times ranging from 1 to 3 weeks. Based on these results, we first wanted to verify the possibility to use a similar method to encapsulate into CCMV cages different oligonucleotides of biological relevance such as siRNA and tRNA whose sequences are made of about 20 and 80 nucleotides, respectively. In order to do so, we used as a starting material Variant 1 (V1), a CCMV construct containing additionally an N-terminal histidine tag, followed by a short linker (Figure 1, Table S3, variant 1). VLPs, stored as capsids in acetate buffer pH 5, were first dialyzed against assembly buffer pH 7.2 (Table S1) and subsequently incubated with oligonucleotides according to a specific mass ratio (oligo: CP 1:6). This procedure indeed resulted in the formation of assembled particles 28 nm in diameter according to a $T = 3$ conformation (Figure S1). Moreover, the assembly process was quite fast, since within 30 min of incubation particles were formed. These oligonucleotide filled nanocages were stable at 4 °C and room temperature. However, when incubated for 15 min at 37 °C aggregation was observed (Figure S2). This effect is most probably a result of the lower stabilizing effect of siRNA and tRNA associated with the oligonucleotides' lengths. To use the CCMV VLPs as oligonucleotide delivery vehicle a more stringent stabilization method was therefore required. This stabilization should however not interfere with oligonucleotide release in the cells. We therefore decided to use the homobifunctional and water-soluble DTSSP (3,3′-dithiobis (sulfosuccinimidylpropionate)) cross-linker. This specific cross-linker is composed of two NHS moieties capable of reacting with primary amines of the lysine side chains leading to covalent amide bonds. In addition, the disulfide bond guarantees cleavage of the cross-links after cellular uptake as a consequence of the high reducing environment of the cytosol.[35,36] We first wanted to assess this strategy on empty nanoparticles. Since NHS-coupling is effective within a pH range of 7−9 we needed to develop a stable CCMV platform at neutral pH. In order to do so we exploited an ELP-CCMV variant well characterized in our research group (Figure 1, Table S3, variant 2).[26−28] It was previously shown that with variant 2 stable particles can be generated in this pH window via Ni-induced assembly exploiting the histidine tag preceding the ELP domain even in the absence of negatively charged cargo.[24,25] We exploited this mechanism in order to form $T = 3$ empty CCMV nanoparticles to test our cross-linking strategy. CCMV assemblies of variant 2 (V2) were generated as follows. V2 particles in their stock solution were dialyzed to pH 5 deprived of EDTA (Table S1, capsid buffer). Subsequently, 10 equiv of nickel chloride dissolved in the same buffer were added to the protein solution with a final CP concentration of

DOI: 10.1021/acs.bioconjchem.9b00731
Bioconjugate Chem. 2019, 30, 3069−3077

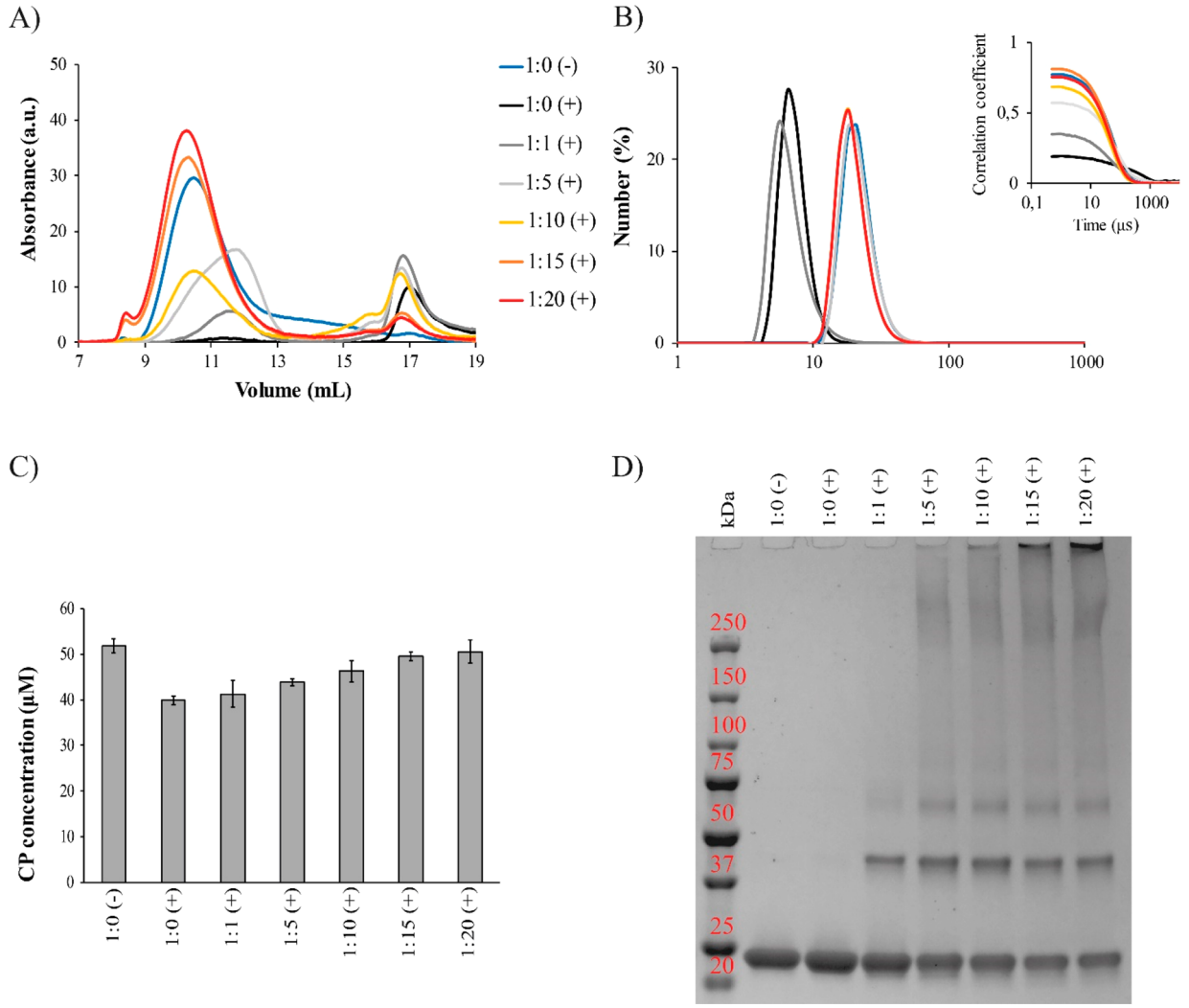

Figure 2. DLS analysis (A), SEC chromatograms (B), UV−visible spectroscopy (C), as well as native SDS-PAGE (D) of V2 nanoparticles in PBS pH 7.2 after cross-linking with DTSSP at different concentrations (1:0, 1:1, 1:5, 1:10, 1:15, and 1:20 CP/DTSSP molar ratio). Nickel-stabilized particles with (+) and without (−) EDTA (2 mM) were used as negative and positive control, respectively. Both the number distribution plot and the absorption spectrum at 280 nm showed stable capsids of 28 nm in diameter in the presence of at least 15:1 molar excess of DTSSP to CP. Increasing DTSSP concentrations resulted in higher particle stability as shown by the CP concentration in solution. Protein bands on gel electrophoresis were visualized with Coomassie staining. Bands associated with unmodified CP appeared at 22 kDa while bands associated with cross-linked dimers and trimers at about 44 and 66 kDa, respectively.

100 μM. After 30 min of incubation, particles were dialyzed to PBS pH 7.2 (Table S1). The obtained product was finally cross-linked with a 1:20 CP: DTSSP molar ratio (50 μM CP concentration) and dialyzed again in PBS (Table S1). Particle size before and after cross-linking was assessed at different stages of this procedure exploiting dynamic light scattering. Moreover, the effect of EDTA (2 mM) on particle stability in the presence of DTSSP was verified. Non-cross-linked nickel-induced $T = 3$ particles disassembled into dimers after addition of the chelating agent. On the contrary, cross-linked particles retained their size of 28 nm (Figure S3).

We optimized the cross-linking conditions by assessing the effect of different DTSSP: CP molar ratios (ranging from 1 to 20 DTSSP molar excess) on particle stability. By simply adding EDTA to the final protein solution we were able to evaluate, using size exclusion chromatography and dynamic light scattering, the cross-linker effect after removal of the stabilizing Ni ions (Figure 2A,B). Both analyses were performed in triplicate. Figure 2A clearly shows that stable particles of 28 nm in diameter, which eluted at 10.2 mL, were generated according to a 15 to 20 molar excess of cross-linker. Smaller peaks eluting at 8.6 mL could be either associated with a lower extent of interparticle cross-linking or impurities in the samples. However, those peaks were sometimes present in our particle solution either before functionalization or after labeling indicating the negligibility of their presence for our stability evaluation. By using a 1:10 CP/DTSSP molar ratio SEC data clearly showed a gradual shift from the dimeric stage, associated with peaks eluting at 17 mL, to capsid formation with increasing concentration of cross-linker. As expected, particles without cross-linker or treated with lower amount of DTSSP were unstable after incubation with EDTA (2 mM). DLS analysis of the same samples is shown in Figure 2B. Stable capsids were obtained employing a CP/DTSSP molar excess of 1:15 and 1:20. Indeed, the correlation coefficient value went back to the original one obtained with stable Ni-induced capsids. The stabilizing effect of DTSSP was further proven by analyzing the protein concentration in solution using UV−

DOI: 10.1021/acs.bioconjchem.9b00731
Bioconjugate Chem. 2019, 30, 3069−3077

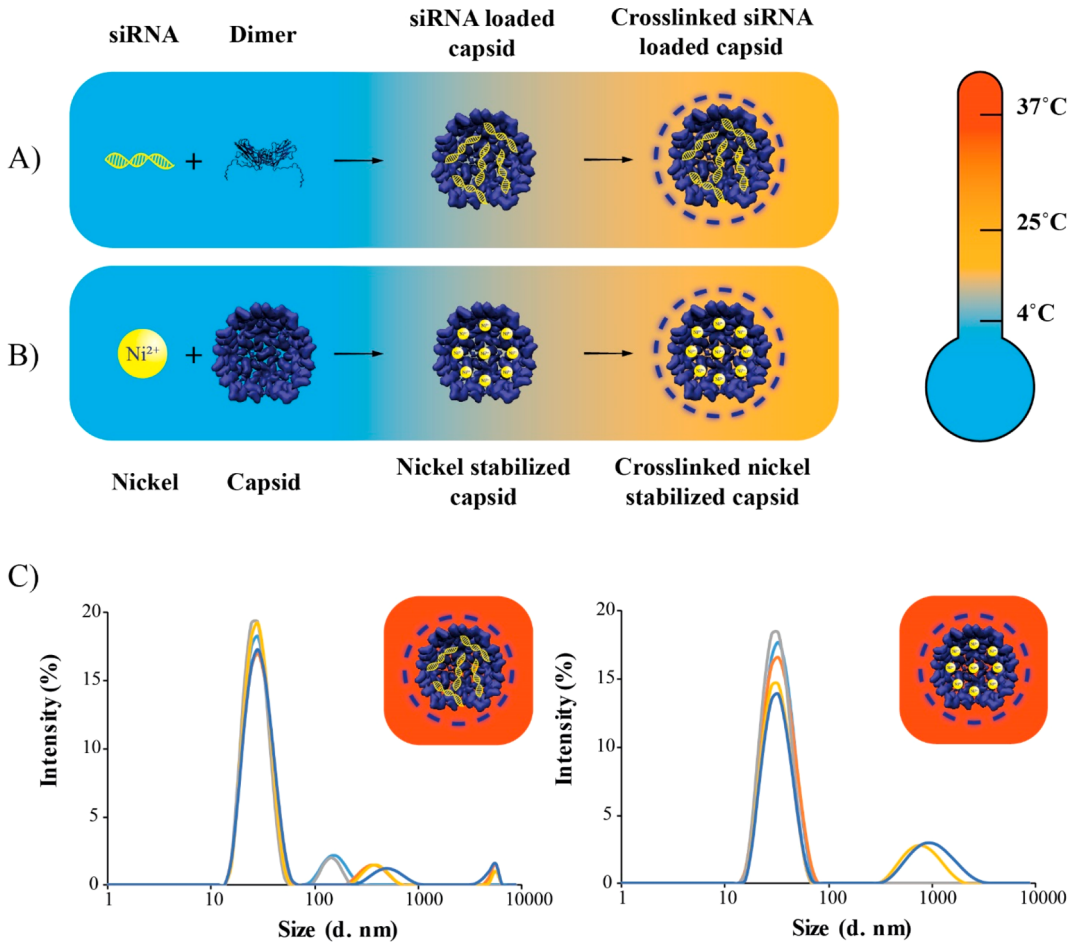

Figure 3. (A) Schematic representation of siRNA-induced V1 particle assembly and capsid cross-linking. The incubation at 4 °C of V1 dimers with oligonucleotides led to capsid formation at neutral pH. Particles were subsequently dialyzed in PBS and cross-linked with a 20:1 DTSSP/CP molar excess at room temperature. (B) Schematic representation of V2 particle stabilization in the presence of Ni followed by capsid cross-linking. The incubation at 4 °C of V2 capsids with Ni led to capsid stabilization. As a consequence, particles could be dialyzed in PBS and cross-linked with a 20:1 DTSSP/CP molar excess at room temperature. (C) DLS analysis of cross-linked siRNA-loaded V1 capsids (left) and cross-linked V2 capsids (right) in PBS after incubation at 37 °C for 0 (light blue), 1 (orange), 2 (gray), 6 (yellow), and 12 (dark blue) hours: (a) Intensity distribution plots show stable particles over time.

visible spectroscopy (Figure 2C). Samples treated with insufficient amounts of cross-linker showed a decrease in protein concentration due to precipitation; only with a 20 molar excess the concentration was maintained at its original value (50 μM CP). To further prove the presence of intermolecular cross-linking between CPs we analyzed samples using gel electrophoresis (Figure 2D). In the absence of a reducing agent, CCMV nanoparticles showed the traditional capsid protein band at 22 kDa after thermal denaturation. On the contrary, an increase in DTSSP concentration induced a decrease of the capsid protein signal and an increase in intensity for bands associated with CP dimers (44 kDa), trimers (66 kDa) as well as larger structures indicating intraparticle cross-linking. Furthermore, the same samples treated with TCEP showed only monomeric bands indicating disulfide bond reduction of DTSSP (Figure S4) Moreover, the comparable intensity of CP bands in the presence of the reducing agent indicates negligible protein aggregation after the cross-linking reaction, in agreement with our previous results. According to our experiments, the 15 to 20 molar excess of cross-linker represents the optimal window for particle functionalization. Higher DTSSP concentration could potentially lead to particle aggregation associated with interparticle cross-linking. We furthermore evaluated the stability of cross-linked particles (20 molar excess of DTSSP) in PBS after 6 h at 25 °C (Figure S5). As expected, cross-linked capsids were stable over time, while Ni-stabilized particles disassembled in the presence of EDTA (2 mM). After having optimized the cross-linking reaction conditions on empty V2 nanoparticles, we next tried to reproduce it exploiting variant 1 (V1), suitable for oligonucleotide encapsulation by employing the arginine-rich domain at the N-terminus of this protein sequence. As shown in Figure S6, a 20 molar excess of cross-linker was sufficient to stabilize siRNA-loaded particles without affecting their size (experiments repeated in triplicate). Moreover, the same strategy was successfully employed for the stabilization of tRNA-loaded nanoparticles involving different CCMV variants presented in this article. Our results showed that the cross-linking of capsid proteins after particle formation was robust and reproducible.

Stability of Cross-Linked Particles under Physiological Conditions. After having developed an efficient cross-linking strategy for particle stabilization at neutral pH, even in the absence of the viral cargo, we wanted to verify the effect of temperature increase on particle stability. We therefore prepared DTSSP-cross-linked samples of V1 and V2 using

DOI: 10.1021/acs.bioconjchem.9b00731
Bioconjugate Chem. 2019, 30, 3069−3077

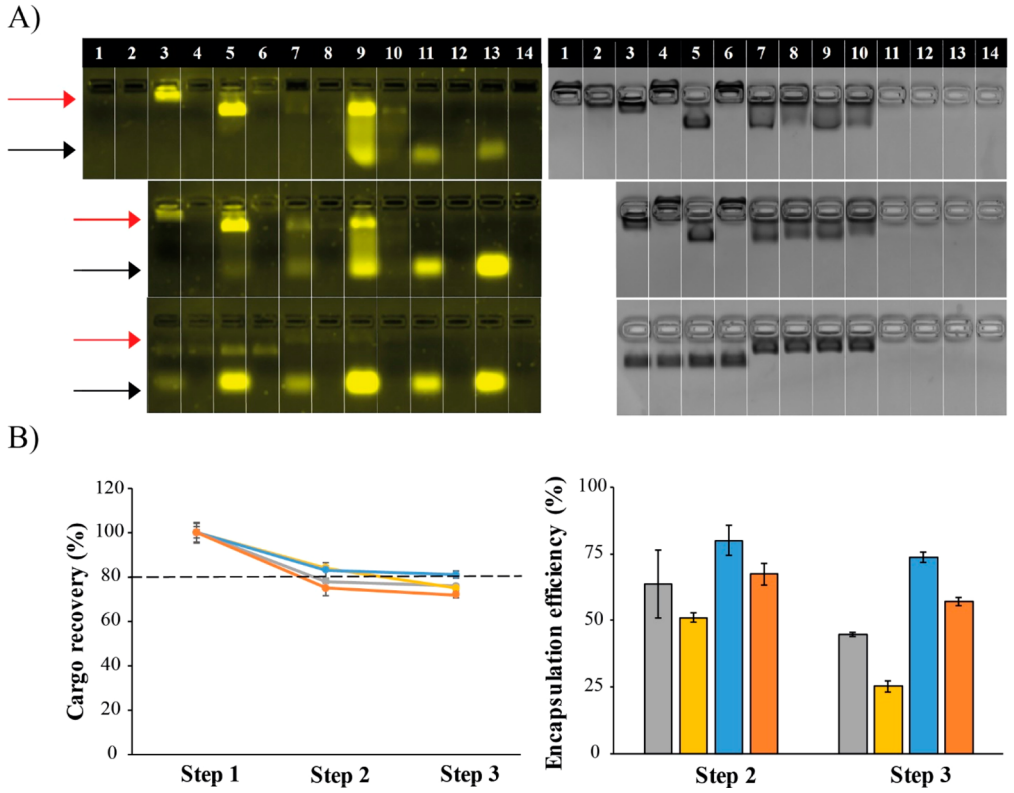

Figure 4. (A) Agarose gel electrophoresis of V1 and V4 nanoparticles loaded with siRNA/tRNA before and after cross-linking as well as after treatment with RNase. V1 particles were generated after incubation of V1 dimers with oligonucleotides. V4 particles were formed after incubation of dimers and oligonucleotides in the presence of Ni. Gels were stained with both SYBR Gold (left) and Coomassie (right). Samples were analyzed in assembly buffer (upper panel), after dialysis in PBS (middle panel), and after the cross-linking reaction with DTSSP (lower panel). 1: V1 dimers, 2: V4 dimers, 3: V1 + tRNA, 4: V1 + tRNA + RNase, 5: V1 + siRNA, 6:V1 + siRNA + RNase, 7: V4 + tRNA, 8: V4 + tRNA + RNase, 9: V4 + siRNA, 10: V4 + siRNA + RNase, 11: tRNA, 12: tRNA + RNase, 13: siRNA, 14: siRNA + RNase. Red and black arrows to the left panel indicate encapsulated oligonucleotides and free siRNA/tRNA respectively. (B) Analysis of cargo recovery (left) as well as encapsulation efficiency (right) of siRNA/tRNA loaded V1 and V4: gray) V1 + siRNA, yellow) V4 + siRNA + Ni, blue) V1 + tRNA, orange) V4 + tRNA + Ni, step 1: oligonucleotide encapsulation in Assembly buffer, step 2: dialysis against PBS, step 3: capsid cross-linking and dialysis in PBS.

the optimized protocol (Figure 3A,B). We incubated particles at 37 °C and analyzed them with DLS at different time intervals. We found that cross-linked particles were strongly stabilized over time and almost no aggregation was observed (Figure 3C). On the contrary, negative controls stabilized with only siRNA (V1) or nickel (V2) were not stable for more than 2 h (Figure S7).

Finally, we wanted to study the effect of a reducing agent such as DTT on particle stability in order to verify the possibility to have particle disassembly inside the cytosol. Within a few minutes of incubation at 37 °C in a PBS solution containing 10 mM DTT, mimicking the reducing environment of the cytoplasm,[35,36] particles were disassembling or aggregating (Figure S8) indicating particle instability in such conditions. As a consequence of the DTSSP stabilizing effect we were able to assess the zeta-potential of our formulation. Native particles usually aggregate during this assay because of their low stability in pure water, making the measurements unreliable. Conversely, DTSSP-CCMV particle size was constant before and after the zeta-potential analysis. The final zeta-potential of cross-linked particles (20 DTSSP molar excess) was -18 ± 3.4 mV (Figure S9).

In a final optimization step, we modified the CCMV sequence to investigate if it could be made more amenable for siRNA binding. It was previously described that the arginine rich domain (ARD) is required for the electrostatic interactions that guarantee cargo-induced assembly, as was also demonstrated with V1.[19,37] Since V2 lacks this specific sequence at the N-terminus, we decided to clone two additional ELP-CCMV variants (Figure 1). Variant 3 was selected as a negative control since it only contains one point mutation at the beginning of the ELP sequence where a leucine is substituted with an arginine. Variant 4 was generated in order to verify the effect of the introduction of an important part of the ARD into the sequence (Table S3). Both variants contained a His tag. First, as a model, yeast tRNA was selected as a probe to evaluate encapsulation by the different variants. Capsid proteins were incubated with the oligonucleotide as described above. As expected, DLS analysis revealed particle formation with variant 1 containing the native ARD which guarantees electrostatic interaction with the negatively charged tRNA (Figure S10A). No particles were observed with variants 2 and 3 since no electrostatic interaction is present, thus making cargo-induced assembly impossible. The last variant (V4) showed an intermediate behavior with a combination of dimers and particles. We then analyzed the effect of Ni addition to the particles in the presence of the tRNA (Figure S10B). While the first variant aggregated, all ELP variants (2, 3, and 4) were able to form well-defined capsids. Agarose gel electrophoresis was performed in order to assess tRNA encapsulation by the ELP-CCMV variants (Figure S11). Encapsulation of oligonucleotides was observed for variant 4

DOI: 10.1021/acs.bioconjchem.9b00731
Bioconjugate Chem. 2019, 30, 3069−3077

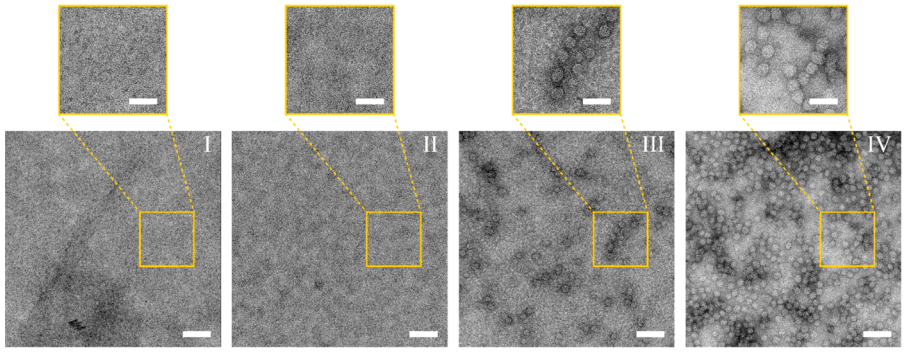

Figure 5. (A) TEM images of CCMV samples, all scale bars indicate 100 and 50 nm in the main images and zoom-in images respectively: (I) V1 dimers in assembly buffer, (II) V1 dimers after incubation with water in assembly buffer, (III) V1 dimers after incubation with siRNA in assembly buffer, and (IV) V1 siRNA-loaded nanoparticles after cross-linking in PBS.

while only free tRNA was observed for the remaining ELP variants (V2 and V3). Based on this evaluation, we decided to perform further experiments using variants 1 and 4 only.

siRNA Loaded Cross-Linked Particles. Particle loading was further investigated exploiting both tRNA and antiluciferase siRNA. Particles of 28 nm in diameter were observed for both variants (V1 and V4), even though the fourth variant required Ni addition as an aid to capsid assembly. In order to have an estimation of the loading efficiency we analyzed particles with agarose gel electrophoresis at three crucial points of particle preparation (Figure 4A); we examined oligonucleotide association with the particles after incubation in assembly buffer as well as after dialysis in PBS and addition of DTSSP. We stained gels with SybrGold and Coomassie in order to visualize both the oligonucleotides and CCMV proteins.

As expected, no oligonucleotide signal was observed for both unloaded CPs (lane 1 and 2). On the contrary, a clear upper band associated with encapsulated oligonucleotides was observed for both loaded variants (lanes 3, 5, 7, and 9). V4 showed less efficient encapsulation compared to V1 as can be noticed from the presence of lower eluting bands associated with free siRNA and tRNA. The tRNA signal was on average less pronounced compared to the one of the siRNA, and this is probably associated with its lower stability. After the cross-linking reaction, the lower bands associated with free oligonucleotides in solution were more pronounced (lanes 3, 5, 7, and 9). Our hypothesis is that part of the oligonucleotides adsorbs at the protein mantle during particle formation. The NHS-coupling of the cross-linker to the lysines on the particle surface could lead to a decrease in electrostatic interactions, inducing a partial tRNA/siRNA release. As an additional control, we added RNase to the same samples in order to evaluate the protecting effect of the protein cages on encapsulated oligonucleotides (lanes 4, 6, 8, and 10). Loaded V1 and V4 nanoparticles before cross-linking were not capable of protecting their cargo. On the other hand, after cross-linking, siRNA and tRNA were fully protected from digestion. As a control, the same RNase concentration was sufficient to fully digest free siRNA and tRNA (lanes 11, 12, 13, and 14). The loading efficiency as well as cargo stability were analyzed combining UV−visible spectroscopy with the fluorescence intensity of the Ribo-green reagent (Figure S12). The former was used in order to monitor oligonucleotide and protein concentrations at 260 and 280 nm during particle assembly and cross-linking. The latter was employed since it represents an accurate quantification method for free oligonucleotides in solution. We analyzed particle and oligonucleotide absorption at the same crucial points described above. Analysis of cargo recovery as well as encapsulation efficiency of siRNA/tRNA loaded V1 and V4 are reported in Figure 4B. Within the first step 17% of the total tRNA incubated with V1 was lost as well as 19% of the total tRNA incubated with V4. A similar trend was observed for the total siRNA incubated with V1 and V4 with a loss of 22% and 24%, respectively. However, in the second step the oligonucleotide loss decreased. We found a 2% reduction on the total tRNA for V1 and 3% for V4. Similar values were recorded for siRNA with a 2% and 9% loss for V1 and V4, respectively. This trend indicates that the cross-linking reaction barely affects oligonucleotide stability and concentration in solution. A loading efficiency of 80% and 63% was estimated for tRNA and siRNA respectively exploiting variant 1. Variant 4 showed a loading efficiency of 68% and 51% for tRNA and siRNA, respectively. After cross-linking, the loading efficiency for V1 dropped to 74% and 45% for tRNA and siRNA, respectively. Variant 4 showed a larger decrease in cargo loading to 57% and 25% for tRNA and siRNA, respectively. Moreover, we estimated the total amount of molecules per virus like particle. About 20 tRNA molecules and 30 siRNA molecules are encapsulated or electrostatically bound in the initial assemblies of V1 CCMV. Variant 4 showed similar values (17 molecules of tRNA and 24 molecules of siRNA per capsid). After cross-linking, about 18 tRNA molecules and 21 siRNA molecules per capsid were still loaded in V1 while in V4 14 and 12 molecules were present, respectively. These data are in agreement with the results obtained with the agarose gel electrophoresis data, and our hypothesis of cross-linking-induced oligonucleotide release from the external side of the capsid. Although both variants proved to be equally capable of encapsulating oligonucleotides into stable capsids, variant 4 still required the presence of nickel ions, which represents an undesirable component for biological applications. For this reason we continued our experiments with variant 1 containing the native CCMV sequence of the virus.

In Vitro Efficacy of Cross-Linked siRNA-Loaded Nanoparticles. After selection of V1 as the therapeutically relevant CCMV delivery vehicle we wanted to verify its efficacy in vitro. We generated siRNA loaded nanoparticles as described above. Before transfection, particle integrity was characterized by TEM. As expected particles (25.8 ± 2.7 nm in diameter) were formed after incubation of V1 dimers with siRNA in the assembly buffer, and their size was maintained

DOI: 10.1021/acs.bioconjchem.9b00731
Bioconjugate Chem. 2019, 30, 3069−3077

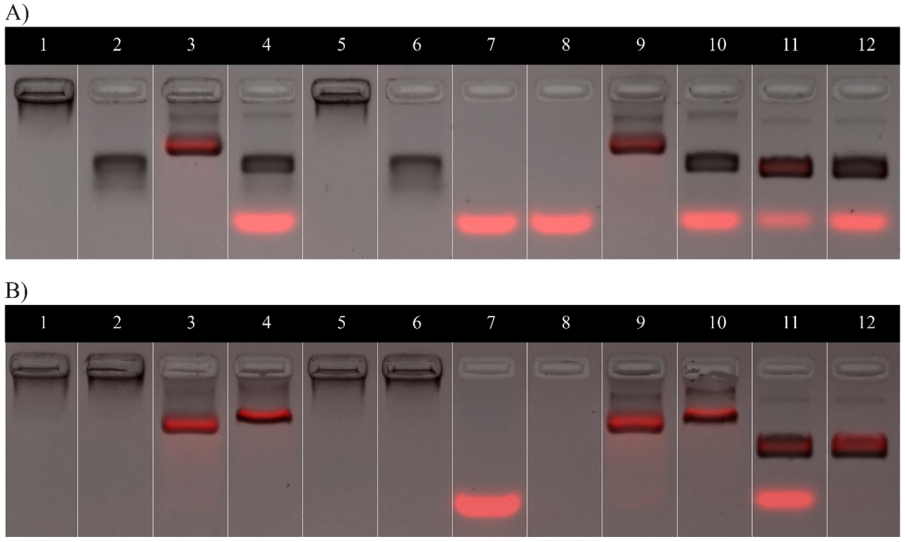

Figure 6. Agarose gel electrophoresis of V1 nanoparticles in the presence (+) or absence (−) of heparin (A) and benzonase (B). Samples were analyzed in assembly buffer (1−8) and PBS (9−12). Coomassie staining (gray) and SYBR gold staining (red) were overlaid. 1: V1 dimer (−), 2: V1 dimer (+), 3: V1 + siRNA (−), 4: V1 + siRNA (+), 5: V1 + H_2O (−), 6: V1 + H_2O (+), 7: siRNA(−), 8: siRNA (+), 9: V1 + siRNA (−), 10: V1 + siRNA (+), 11: cross-linked V1+siRNA (−), 12: cross-linked V1+siRNA. When the siRNA was encapsulated into V1 nanoparticles SYBR Gold staining and Coomassie staining overlapped. Free siRNA appears as a lower red band on the gels. After treatment with heparin, siRNA was released from V1 nanoparticles. After treatment with benzonase, encapsulated siRNA was partially degraded when particles were not cross-linked while it was fully protected inside cross-linked particles.

after cross-linking in PBS (Figure 5). Moreover, particles were incubated with heparin in order to verify the possibility of siRNA release (Figure 6A). Heparin, as it is negatively charged, is capable of penetrating particles, thereby displacing loaded siRNA. This effect was indeed visible for both cross-linked and un-cross-linked particles. Furthermore, we used enzymatic digestion in order to remove all residual free siRNA in solution prior to transfection (Figure 6B).

In vitro experiments were performed exploiting HeLa-luc cells naturally expressing the luciferase enzyme. After addition of the specific luciferin substrate, this enzyme is responsible for luciferin conversion into oxyluciferin with the subsequent emission of light. In the presence of antiluciferase siRNA, the enzyme expression is reduced and the luminescent signal is not generated anymore. We analyzed transfection efficiency using Lipofectamine-2000 and the luciferase assay system (Promega) according to manufacturer's instructions (see methods; Figure 7A). Briefly, HeLa-luc cells were incubated overnight with our samples and Lipofectamine in OptiMEM transfection medium. Afterward, the cell medium was replaced by complete medium and the cells were incubated again for 2 days. Finally, cells were washed and lysed. The substrate was added and the luminescence signal recorded on a multiplate reader. We used medium and free siRNA without lipofectamine as negative controls. Indeed, the maximum luminescence signal was recorded with both samples, since no gene silencing was possible. Both siRNA complexed with lipofectamine, and siRNA loaded V1 nanoparticles treated with lipofectamine were able to transfect cells inducing a knock down effect on luminescence. However, the same samples treated with benzonase (a nuclease) showed completely different behavior. While the lipofectamine complexed siRNA was fully degraded after addition of the enzyme, the VLP encapsulated one was protected and preserved and remained active. Samples used for transfection were further analyzed by TEM (Figure 7B). Particle shape and size were not affected by the addition of lipofectamine or benzonase proving again particle stability in physiological conditions. Even though lipofectamine still is required for efficient transfection of siRNA-loaded CCMV, the easiness of manufacturing together with the high encapsulation efficiency as well as the cargo protection against degradation make this system extremely appealing for oligonucleotide delivery applications. In addition, the high thermal stability conferred by the cross-linker at physiological pH guaranties a higher intracellular release of intact nanoparticles, thus increasing cargo bioavailability. Moreover, particle cross-linking followed by functionalization with a cell penetrating peptide could potentially lead to a drastic increase in particle transfection efficacy in the absence of Lipofectamine.

CONCLUSIONS

We extensively analyzed and characterized a versatile cross-linking strategy in order to stabilize CCMV nanoparticles after cargo loading to make them suitable for efficient in vitro siRNA delivery. We exploited the reducible DTSSP cross-linker in order to conjugate lysines on the particle surface, thereby creating a reversibly cross-linked system that preserves particle integrity. A range of different CCMV variants was analyzed for their stability at physiological conditions and loading capacity. After optimizing the reaction conditions the His-tagged native form of the virus capsid protein (variant 1) proved to give the most promising features. The cross-linked particles were stable at physiological conditions at 37 °C over time, in contrast to the un-cross-linked variant, and they were effectively loaded with an encapsulation efficiency of 74% and 45% for tRNA and siRNA, respectively. We showed that particles loaded with antiluciferase siRNA can efficiently knock down protein expression in the presence of lipofectamine. The addition of a nuclease had no effect on gene silencing efficiency, whereas siRNA complexed with lipofectamine was completely degraded under the same conditions. We think that our siRNA loaded and cross-linked CCMV platform is highly

DOI: 10.1021/acs.bioconjchem.9b00731
Bioconjugate Chem. 2019, 30, 3069−3077

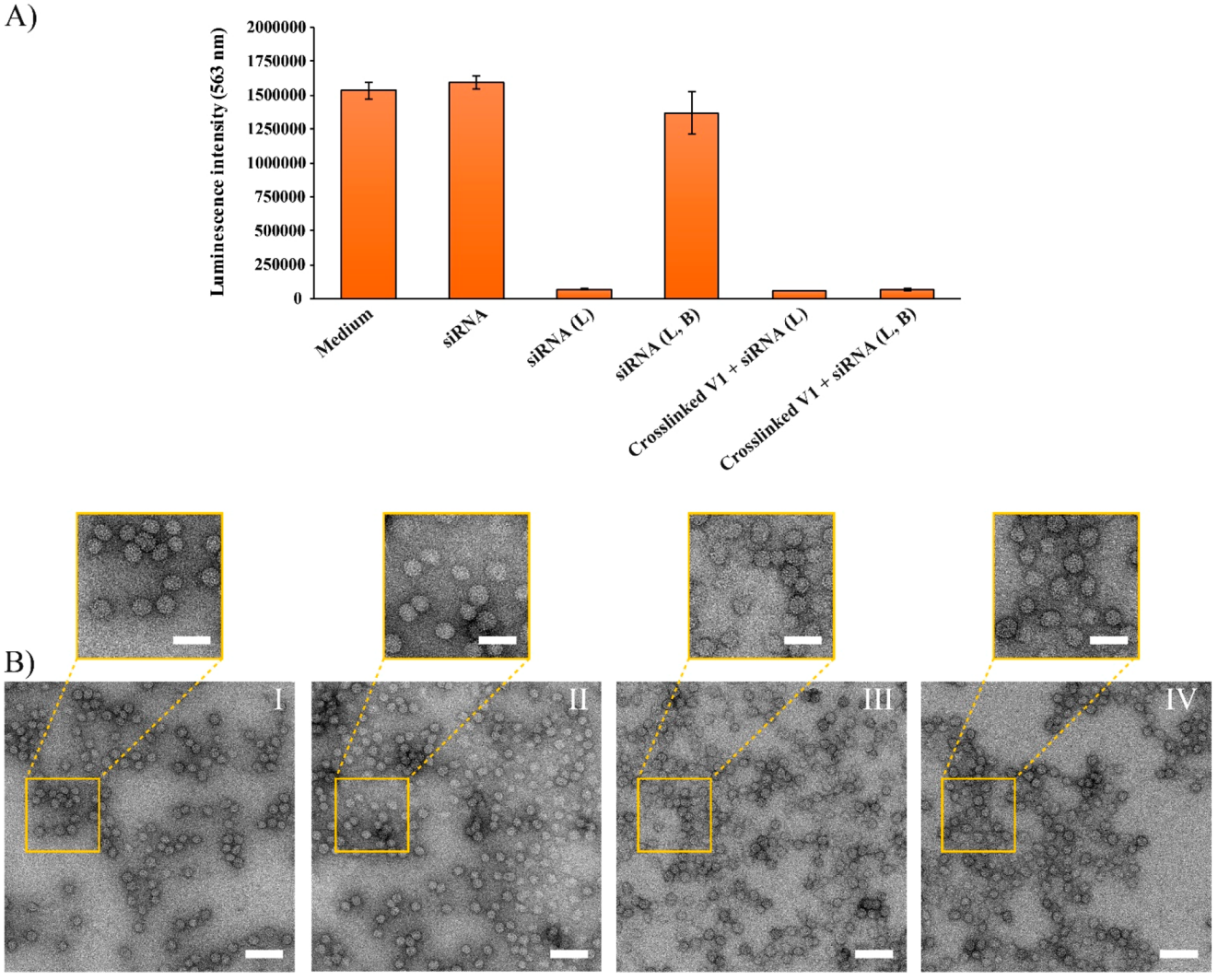

Figure 7. (A) Luciferase assay with HeLa-Luc cell line. Transfection efficacy of siRNA and cross-linked siRNA-loaded V1 nanoparticles in the presence or absence of benzonase (B) and Lipofectamine (L); (B) TEM images of CCMV samples in OptiMEM, all scale bars indicate 100 and 50 nm in the main images and zoom-in images, respectively: (I) siRNA-loaded V1 nanoparticles, (II) siRNA-loaded V1 nanoparticles treated with benzonase, (III) siRNA loaded V1 nanoparticles after incubation with lipofectamine, and (IV) siRNA-loaded V1 nanoparticles after incubation with both benzonase and lipofectamine.

suitable for gene delivery applications; furthermore our reversible cross-linking method greatly widens the application scope of CCMV particles to many types of drug delivery.

■ ASSOCIATED CONTENT

Supporting Information

The Supporting Information is available free of charge at https://pubs.acs.org/doi/10.1021/acs.bioconjchem.9b00731.

Experimental methods as well as figures and tables (PDF)

■ AUTHOR INFORMATION

Corresponding Author

*E-mail: J.C.M.v.Hest@tue.nl.

ORCID

Jan C. M. van Hest: 0000-0001-7973-2404

Notes

The authors declare no competing financial interest.

■ ACKNOWLEDGMENTS

This project has received funding from the European Union's Horizon 2020 research and innovation programme under the Marie Skłodowska-Curie Grant Agreement No. 722717. We thank Johan F. J. Engbersen, Dennis Lensen, and 20 Med Therapeutics for the fruitful collaboration. The authors acknowledge Daan Vervoort, Suzanne Timmermans, and Lise Schoonen for their motivating and helpful comments.

■ REFERENCES

(1) Zhang, L., Gu, F. X., Chan, J. M., Wang, A. Z., Langer, R. S., and Farokhzad, O. C. (2008) Nanoparticles in medicine: therapeutic applications and developments. *Clin. Pharmacol. Ther. 83*, 761−769.

(2) Douglas, T., and Young, M. (2006) Viruses: making friends with old foes. *Science 312*, 873−875.

(3) Rohovie, M. J., Nagasawa, M., and Swartz, J. R. (2017) Virus-like particles: Next-generation nanoparticles for targeted therapeutic delivery. *Bioeng. Transl. Med. 2*, 43−57.

(4) Putri, R. M., Cornelissen, J. J., and Koay, M. S. (2015) Self-Assembled Cage-Like Protein Structures. *ChemPhysChem 16*, 911−918.

DOI: 10.1021/acs.bioconjchem.9b00731
Bioconjugate Chem. 2019, 30, 3069−3077

(5) Uchida, M., Klem, M. T., Allen, M., Suci, P., Flenniken, M., Gillitzer, E., Varpness, Z., Liepold, L. O., Young, M., and Douglas, T. (2007) Biological containers: protein cages as multifunctional nanoplatforms. *Adv. Mater. 19*, 1025−1042.
(6) Schoonen, L., and van Hest, J. C. (2014) Functionalization of protein-based nanocages for drug delivery applications. *Nanoscale 6*, 7124−7141.
(7) Steinmetz, N. F. (2010) Viral nanoparticles as platforms for next-generation therapeutics and imaging devices. *Nanomedicine 6*, 634−641.
(8) Lam, P., and Steinmetz, N. F. (2019) Delivery of siRNA therapeutics using cowpea chlorotic mottle virus-like particles. *Biomater. Sci. 7*, 3138−3142.
(9) Azizgolshani, O., Garmann, R. F., Cadena-Nava, R., Knobler, C. M., and Gelbart, W. M. (2013) Reconstituted plant viral capsids can release genes to mammalian cells. *Virology 441*, 12−17.
(10) Lam, P., and Steinmetz, N. F. (2018) Plant viral and bacteriophage delivery of nucleic acid therapeutics. *Wiley Interdiscip. Rev. Nanomedicine Nanobiotechnology 10*, e1487.
(11) Caspar, D. L., and Klug, A. (1962) Physical principles in the construction of regular viruses. *Cold Spring Harbor Symp. Quant. Biol. 27*, 1−24.
(12) Speir, J. A., Munshi, S., Wang, G., Baker, T. S., and Johnson, J. E. (1995) Structures of the native and swollen forms of cowpea chlorotic mottle virus determined by X-ray crystallography and cryo-electron microscopy. *Structure 3*, 63−78.
(13) Comellas-Aragonès, M., Sikkema, F. D., Delaittre, G., Terry, A. E., King, S. M., Visser, D., Heenan, R. K., Nolte, R. J. M., Cornelissen, J. J. L. M., and Feiters, M. C. (2011) Solution scattering studies on a virus capsid protein as a building block for nanoscale assemblies. *Soft Matter 7*, 11380−11391.
(14) Fox, J. M., Wang, G., Speir, J. A., Olson, N. H., Johnson, J. E., Baker, T. S., and Young, M. J. (1998) Comparison of the native CCMV virion within vitroassembled CCMV virions by cryoelectron microscopy and image reconstruction. *Virology 244*, 212−218.
(15) Liepold, L. O., Revis, J., Allen, M., Oltrogge, L., Young, M., and Douglas, T. (2005) Structural transitions in Cowpea chlorotic mottle virus (CCMV). *Phys. Biol. 2*, S166.
(16) Zhao, X., Fox, J. M., Olson, N. H., Baker, T. S., and Young, M. J. (1995) In vitro assembly of cowpea chlorotic mottle virus from coat protein expressed in Escherichia coli and in vitro-transcribed viral cDNA. *Virology 207*, 486−494.
(17) Fox, J. M., Zhao, X., Speir, J. A., and Young, M. J. (1996) Analysis of a salt stable mutant of cowpea chlorotic mottle virus. *Virology 222*, 115−122.
(18) Zhang, J., Baker, M. L., Schröder, G. F., Douglas, N. R., Reissmann, S., Jakana, J., Dougherty, M., Fu, C. J., Levitt, M., Ludtke, S. J., Chiu, W., and Frydman, J. (2010) Mechanism of folding chamber closure in a group II chaperonin. *Nature 463*, 379−383.
(19) Garmann, R. F., Comas-Garcia, M., Koay, M. S., Cornelissen, J. J., Knobler, C. M., and Gelbart, W. M. (2014) Role of electrostatics in the assembly pathway of a single-stranded RNA virus. *J. Virol. 88*, 10472−10479.
(20) Hu, Y., Zandi, R., Anavitarte, A., Knobler, C. M., and Gelbart, W. M. (2008) Packaging of a polymer by a viral capsid: the interplay between polymer length and capsid size. *Biophys. J. 94*, 1428−1436.
(21) Minten, I. J., Ma, Y., Hempenius, M. A., Vancso, G. J., Nolte, R. J., and Cornelissen, J. J. (2009) CCMV capsid formation induced by a functional negatively charged polymer. *Org. Biomol. Chem. 7*, 4685−4688.
(22) Cadena-Nava, R. D., Hu, Y., Garmann, R. F., Ng, B., Zelikin, A. N., Knobler, C. M., and Gelbart, W. M. (2011) Exploiting fluorescent polymers to probe the self-assembly of virus-like particles. *J. Phys. Chem. B 115*, 2386−2391.
(23) Kwak, M., Minten, I. J., Anaya, D. M., Musser, A. J., Brasch, M., Nolte, R. J., Müllen, K., Cornelissen, J. J. L. M., and Herrmann, A. (2010) Virus-like particles templated by DNA micelles: a general method for loading virus nanocarriers. *J. Am. Chem. Soc. 132*, 7834−7835.
(24) van Eldijk, M. B., Schoonen, L., Cornelissen, J. J., Nolte, R. J., and van Hest, J. C. (2016) Metal Ion-Induced Self-Assembly of a Multi-Responsive Block Copolypeptide into Well-Defined Nanocapsules. *Small 12*, 2476−2483.
(25) Schoonen, L., Maassen, S., Nolte, R. J., and van Hest, J. C. (2017) Stabilization of a virus-like particle and its application as a nanoreactor at physiological conditions. *Biomacromolecules 18*, 3492−3497.
(26) Timmermans, S. B., Vervoort, D. F., Schoonen, L., Nolte, R. J., and van Hest, J. C. (2018) Self-Assembly and Stabilization of Hybrid Cowpea Chlorotic Mottle Virus Particles under Nearly Physiological Conditions. *Chem. - Asian J. 13*, 3518−3525.
(27) Schoonen, L., Maas, R. J., Nolte, R. J., and van Hest, J. C. (2017) Expansion of the assembly of cowpea chlorotic mottle virus towards non-native and physiological conditions. *Tetrahedron 73*, 4968−4971.
(28) van Eldijk, M. B., Wang, J. C. Y., Minten, I. J., Li, C., Zlotnick, A., Nolte, R. J., Cornelissen, J. J. L. M., and van Hest, J. C. (2012) Designing two self-assembly mechanisms into one viral capsid protein. *J. Am. Chem. Soc. 134*, 18506−18509.
(29) Schoonen, L., Pille, J., Borrmann, A., Nolte, R. J., and van Hest, J. C. (2015) Sortase A-mediated N-terminal modification of cowpea chlorotic mottle virus for highly efficient cargo loading. *Bioconjugate Chem. 26*, 2429−2434.
(30) Comellas-Aragonès, M., Engelkamp, H., Claessen, V. I., Sommerdijk, N. A., Rowan, A. E., Christianen, P. C., Maan, J. C., Verduin, B. J. M., Cornelissen, J. J. L. M., and Nolte, R. J. (2007) A virus-based single-enzyme nanoreactor. *Nat. Nanotechnol. 2*, 635.
(31) de Ruiter, M. V., Putri, R. M., and Cornelissen, J. J. (2018) CCMV-based enzymatic nanoreactors. *Methods Mol. Biol. 1776*, 237−247.
(32) Maassen, S. J., de Ruiter, M. V., Lindhoud, S., and Cornelissen, J. J. (2018) Oligonucleotide Length-Dependent Formation of Virus-Like Particles. *Chem. - Eur. J. 24*, 7456−7463.
(33) Cadena-Nava, R. D., Comas-Garcia, M., Garmann, R. F., Rao, A. L. N., Knobler, C. M., and Gelbart, W. M. (2012) Self-assembly of viral capsid protein and RNA molecules of different sizes: requirement for a specific high protein/RNA mass ratio. *J. Virology 86*, 3318−3326.
(34) Garmann, R. F., Comas-Garcia, M., Knobler, C. M., and Gelbart, W. M. (2016) Physical principles in the self-assembly of a simple spherical virus. *Acc. Chem. Res. 49*, 48−55.
(35) Cheng, R., Feng, F., Meng, F., Deng, C., Feijen, J., and Zhong, Z. (2011) Glutathione-responsive nano-vehicles as a promising platform for targeted intracellular drug and gene delivery. *J. Controlled Release 152*, 2−12.
(36) Bauhuber, S., Hozsa, C., Breunig, M., and Göpferich, A. (2009) Delivery of nucleic acids via disulfide-based carrier systems. *Adv. Mater. 21*, 3286−3306.
(37) Tan, R., and Frankel, A. D. (1995) Structural variety of arginine-rich RNA-binding peptides. *Proc. Natl. Acad. Sci. U. S. A. 92*, 5282−5286.

DOI: 10.1021/acs.bioconjchem.9b00731
Bioconjugate Chem. 2019, 30, 3069−3077